Subcellular targeting of oxidants during endothelial cell migration

Ru Feng Wu,[1] You Cheng Xu,[1] Zhenyi Ma,[1] Fiemu E. Nwariaku,[1] George A. Sarosi Jr.,[1,2] and Lance S. Terada[1,2]

[1]University of Texas Southwestern, Dallas, TX 75390
[2]Dallas Veterans Administration Medical Center, Dallas, TX 75390

Endogenous oxidants participate in endothelial cell migration, suggesting that the enzymatic source of oxidants, like other proteins controlling cell migration, requires precise subcellular localization for spatial confinement of signaling effects. We found that the nicotinamide adenine dinucleotide phosphate reduced (NADPH) oxidase adaptor $p47^{phox}$ and its binding partner TRAF4 were sequestered within nascent, focal complexlike structures in the lamellae of motile endothelial cells. TRAF4 directly associated with the focal contact scaffold Hic-5, and the knockdown of either protein, disruption of the complex, or oxidant scavenging blocked cell migration. An active mutant of TRAF4 activated the NADPH oxidase downstream of the Rho GTPases and p21-activated kinase 1 (PAK1) and oxidatively modified the focal contact phosphatase PTP-PEST. The oxidase also functioned upstream of Rac1 activation, suggesting its participation in a positive feedback loop. Active TRAF4 initiated robust membrane ruffling through Rac1, PAK1, and the oxidase, whereas the knockdown of PTP-PEST increased ruffling independent of oxidase activation. Our data suggest that TRAF4 specifies a molecular address within focal complexes that is targeted for oxidative modification during cell migration.

Introduction

Migrating cells engage in the cyclic formation and dissolution of points of contact between the lamellipodium and the matrix, creating transitory integrin clusters termed focal complexes (Nobes and Hall, 1995). Although generally smaller than mature focal adhesions, leading edge focal complexes bear the strongest tensile forces in migrating cells (Beningo et al., 2001). In theory, the turnover of focal complexes at the leading edge may be necessary for the constantly remodeling lamellipodium to simultaneously translocate forward while also retaining the ability to retract and change direction based on matrix sampling or soluble chemoattractant gradients. Accordingly, interventions that either interrupt or stabilize focal complex formation impair normal cell migration (Rottner et al., 1999; Totsukawa et al., 2004; Webb et al., 2004). These same interventions may also diminish membrane ruffling, suggesting that the latter may occur from tension applied to segments of lamellipodia that are transiently unanchored as a result of regionally high focal complex turnover.

Focal complex dynamics, in turn, appear to be coordinated by the Rho family of small GTPases. Whereas Rac1 and Cdc42 promote focal complex formation within lamellipodia and filopodia, RhoA facilitates the maturation of focal complexes into stable focal adhesions (Nobes and Hall, 1995; Rottner et al., 1999). To fully polarize these events in the motile cell so that meaningful locomotion can occur, positive feedback loops are initiated, resulting in the rapid amplification of Rho GTPase and p21-activated kinase 1 (PAK1) activation at the leading edge and, thus, asymmetric formation of a lamellipodium (Li et al., 2003). The mechanism by which the small GTPases control focal contact behavior is incompletely understood, but it involves the initiation of protein tyrosine phophorylation events leading to intense tyrosine phosphorylation of focal contact proteins. Rac1 and RhoA, for instance, direct the tyrosine kinase Src to lamellipodia and focal adhesions, respectively, to cause remodeling of these integrin-containing structures (Timpson et al., 2001; Webb et al., 2004). Src, in turn, facilitates full activation of the related focal adhesion tyrosine kinase (Pyk2), and both tyrosine kinases are required for the phosphorylation of a number of focal complex proteins. Opposing these effects, the protein tyrosine phosphatase PTP-PEST is also directed to nascent integrin clusters, where it dephosphorylates and thus inactivates Pyk2 (Lyons et al., 2001; Sastry et al., 2002). Furthermore, PTP-PEST suppresses

Correspondence to Lance S. Terada: Lance.Terada@med.va.gov

Abbreviations used in this paper: 5′-IAF, 5′-iodoacetamidofluorescein; CRIB, Cdc42–Rac1 interaction binding; HUVEC, human umbilical vein endothelial cell; JNK, c-Jun NH_2-terminal kinase; MOI, multiplicity of infection; PAK, p21-activated kinase; PID, PAK inhibitory domain; siRNA, short inhibitory RNA; TIRF, total internal reflection fluorescence.

The online version of this article contains supplemental material.

The Journal of Cell Biology, Vol. 171, No. 5, December 5, 2005 893–904
http://www.jcb.org/cgi/doi/10.1083/jcb.200507004

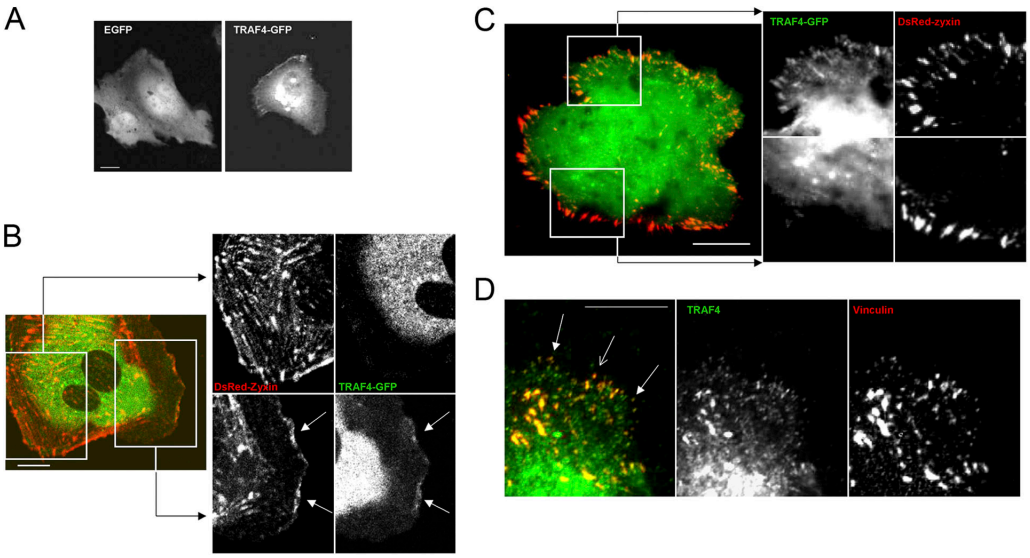

Figure 1. **TRAF4 accumulates in focal complexes.** HUVECs were transfected with the indicated plasmids (color of font indicates pseudocolor designation), plated on fibronectin-coated coverslips, and examined live without fixation using confocal (A and B) or TIRF (C) microscopy. (A) TRAF4-GFP translocated to the tips of leading edges (right), a pattern not seen with pEGFP (left). (B) HUVECs were cotransfected with TRAF4-GFP and DsRed-zyxin. Insets show appearance of TRAF4-GFP and DsRed-zyxin in discontinuous structures at the leading (right) edge of a large protrusion (arrows). Larger stress fiber–anchored focal adhesions contain DsRed-zyxin but no detectable TRAF4-GFP (top insets). (C) TIRF microscopy image of TRAF4-GFP and DsRed-zyxin showing ventral location of small TRAF4-GFP and DsRed-zyxin focal complexes at an advancing protrusion (top inset). Larger DsRed-zyxin focal adhesions lacked TRAF4-GFP (bottom inset). (D) Immunofluorescent images of fixed cells were obtained using TIRF microscopy showing colocalization of endogenous TRAF4 (labeled with AlexaFluor488) within small (closed head arrows) to medium (open head arrow)-sized vinculin aggregates (AlexaFluor555) appearing at the edge of a protrusion. Bars (A–C), 20 μm; (D) 10 μm.

Rac1 activation at the leading edge, diminishing the polarization of migrating cells (Sastry et al., 2002). Although PTP-PEST is thought to target focal contacts through direct binding to paxillin and the paxillin paralogue Hic-5, the mechanism by which its activity is regulated is unclear.

Besides controlling focal complexes and lamellipodia at the leading edge of cells, Rac1 is necessary for activation of the NADPH oxidase. Recently, this oxidase was shown to mediate endothelial cell migration in a Rac1-dependent manner (Moldovan et al., 2000; Ushio-Fukai et al., 2002). Oxidant activity was noted to localize to membrane ruffles (Moldovan et al., 2000), suggesting that distinct functions of Rac1—oxidase activation and control of lamellipodial dynamics—may be spatially and functionally coordinated at the leading edge of migrating cells. Such physical targeting of a tightly regulated oxidant source would present a logical explanation for the observed specificity of oxidant signaling in response to migratory stimuli, circumventing the rapid diffusion and limited target specificity of oxidant molecules themselves. Therefore, we sought to identify molecular targeting devices that may specify the site of oxidant production and, thereby, focus their effects.

We previously reported that the orphan adaptor TRAF4 directly binds the NADPH oxidase subunit $p47^{phox}$ and controls activation of the c-Jun NH_2-terminal kinase (JNK) MAPK (Xu et al., 2002). Notably, mice lacking TRAF4 display defective branchial somite and neural tube closure, and flies lacking the orthologous dTRAF1 fail to activate JNK and complete dorsal closure; both phenotypes suggest abnormal migration (Regnier et al., 2002; Cha et al., 2003). In this study, we found that both TRAF4 and $p47^{phox}$ target focal complexes in association with Hic-5 and initiate Rho GTPase signaling. TRAF4-directed oxidant production selectively targets the redox-sensitive phosphatase PTP-PEST and may participate in a positive feedback cycle that facilitates Rac1 activation.

Results

TRAF4 and $p47^{phox}$ concentrate in focal complexes

In spontaneously migrating endothelial cells, the distribution of TRAF4-GFP was polarized, concentrating in small discontinuous patches near the lamellipodial edge (Fig. 1 A). Because this pattern resembles that of focal complexes, we examined the colocalization of TRAF4 with zyxin, a scaffolding protein that appears in focal complexes and also accumulates in focal adhesions (Krylyshkina et al., 2003; Franco et al., 2004; Totsukawa et al., 2004). By confocal microscopy, TRAF4-GFP was found to localize within discrete, peripheral DsRed-zyxin aggregates of variable size at the leading edge of endothelial cell lamellar protrusions (Fig. 1 B), along occasional microspike shafts and tips, and discontinuously in a peripheral rim around newly adherent cells, which is consistent with focal complex association (Fig. S1, available at http://www.jcb.org/cgi/content/full/jcb.200507004/DC1). In contrast, TRAF4-GFP accumulation in stable stress fiber–associated focal adhesions was weak or absent (Fig. 1 B). The ventral location of TRAF4-GFP was assessed using total internal reflection fluorescence (TIRF) microscopy, which narrows the z-axis resolution to within 100–150 nm of the coverslip surface. Relatively nonpolarized cells showed accurate colocalization of TRAF4-GFP with

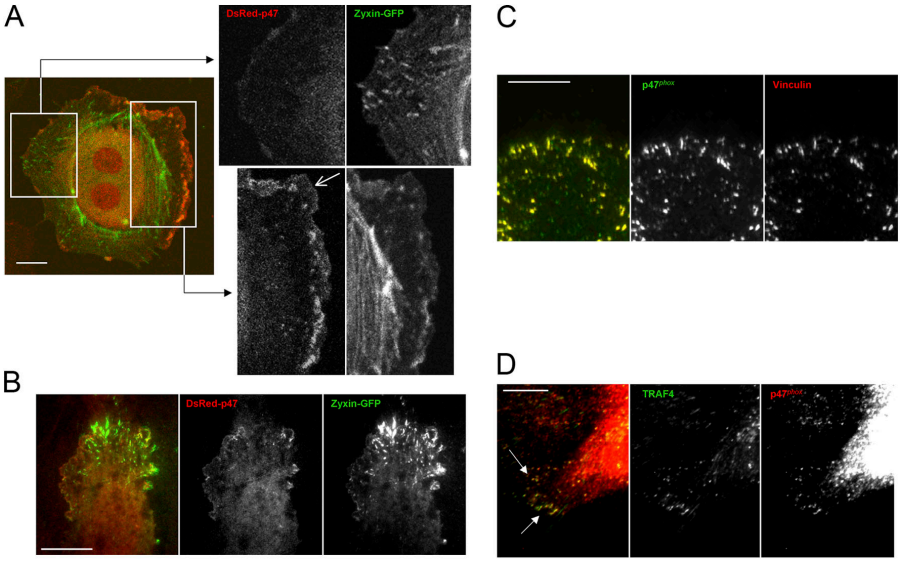

Figure 2. **p47^{phox} associates with TRAF4 in focal complexes.** (A) Confocal image of DsRed-p47 in small, discrete zyxin-GFP–containing complexes within the leading (right) lamellar edge. Stress fiber–associated focal adhesions (top inset) lack DsRed-p47. DsRed-p47 also localized to the periphery (arrow). (B) TIRF image shows ventral appearance of DsRed-p47 with nascent zyxin-GFP aggregates at the leading edge of a protrusion. (C) Immunofluorescent image of endogenous p47^{phox} (AlexaFluor488) showing colocalization with small vinculin (AlexaFluor555) accumulations. (D) Immunofluorescent image showing the appearance of endogenous TRAF4 (AlexaFluor488) and p47^{phox} (AlexaFluor633) in small dotlike structures at the edge of a protrusion (arrows). B–D, TIRF images. Bars (A and B), 20 μm; (C and D) 10 μm.

peripheral DsRed-zyxin aggregates, confirming targeting to juxtamembrane structures (Fig. S2). In more polarized motile cells, TRAF4-GFP preferentially associated with nascent DsRed-zyxin clusters of variable size at the active leading edge of lamellae, but much less so with larger, rearward focal adhesions (Fig. 1 C). In parallel, immunofluorescent images demonstrated colocalization of endogenous TRAF4 to small (≤1 μm) vinculin-containing structures at the edge of human umbilical vein endothelial cell (HUVEC) protrusions, which is again consistent with its early appearance in focal complexes (Fig. 1 D).

The distribution of DsRed-p47 also became highly polarized in migrating endothelial cells, concentrating in zyxin-containing structures within lamellar protrusions (Fig. 2 A). In addition, faint linear accumulation of DsRed-p47 was frequently seen at the outer edge of protrusions before visible organization of zyxin-GFP aggregates. DsRed-p47 was not found within stable focal adhesions in either mobile or static cells. TIRF microscopy also revealed the early appearance of DsRed-p47 at both linear and dotlike ventral structures at the periphery of advancing edges, partially coinciding with zyxin-GFP accumulation (Fig. 2 B). In addition, p47^{phox} specifically coprecipitated with GFP-zyxin (not depicted), which is consistent with its incorporation into focal complex assemblies. By immunofluorescence, endogenous p47^{phox} accurately colocalized with small- to medium-sized vinculin aggregates (Fig. 2 C), and p47^{phox} colocalized with endogenous TRAF4 at the tips of protrusions, which is again consistent with an association within focal complexes (Fig. 2 D).

TRAF4 binds the focal contact protein Hic-5

Using full-length TRAF4 as a Gal4-binding domain bait fusion in a yeast two-hybrid screen, two clones were retrieved from an endothelial cell Gal4 activation domain library (Xu et al., 2002) containing residues 45–444 of Hic-5, including the three LD motifs and four COOH-terminal LIM domains. Yeast mating studies demonstrated interactions between p47^{phox} and TRAF4 and TRAF4 and Hic-5 but not between p47^{phox} and Hic-5 (unpublished data). Binding of TRAF4 to Hic-5 was direct, as indicated by specific pull down of in vitro translated Hic-5 by GST-TRAF4 (Fig. 3 A). Ectopically expressed TRAF4 and Hic-5 cross-coimmunoprecipitated in Phoenix-293 cells (Fig. 3 B), and endogenous TRAF4 coimmunoprecipitated with endogenous Hic-5 in lung microvascular endothelial cells (Fig. 3 C).

Hic-5, like its paralogue paxillin, is directed to focal adhesions through interaction with focal contact proteins. Unlike paxillin, Hic-5 has been demonstrated to have a stronger physical and functional association with the kinase scaffold Pyk2 (related focal adhesion tyrosine kinase CAKβ), which is known to target focal complexes (Litvak et al., 2000), than with the related kinase FAK (Osada et al., 2001). Immunoprecipitation of endogenous Pyk2 brought down detectable amounts of endogenous TRAF4 and Hic-5 (Fig. 3 C), which is consistent with an association of the three focal complex proteins. In addition, Pyk2 coprecipitated ectopically expressed wild-type p47^{phox} and, to a greater extent, the active (open conformation) mutant p47(S303D,S304D,S328D) (Wu et al., 2003) but not the inactive SH3 surface-disrupted mutant p47(W193R) (Fig. 3 D), suggesting that formation of the complex may be associated with the activation state of the oxidase. By TIRF microscopy, DsRed-TRAF4 was found within some but not all Hic-5–GFP focal accumulations (Fig. 3 E). Immunofluorescent stains demonstrated the association of endogenous Hic-5 with vinculin aggregates of various sizes, confirming an association with focal contact structures (Fig. 3 F). Finally, triple labeling studies confirmed the colocalization of endogenous Hic-5 and TRAF4 within small- to medium-sized vinculin aggregates at the periphery of lamellipodia (Fig. 3 G).

TRAF4–Hic-5 interactions control cell migration

Because focal complex formation is critical to cell migration, we next asked whether TRAF4–Hic-5 interactions were important for such migration. First, we found that short inhibitory RNA (siRNA)–mediated knockdown of either endogenous

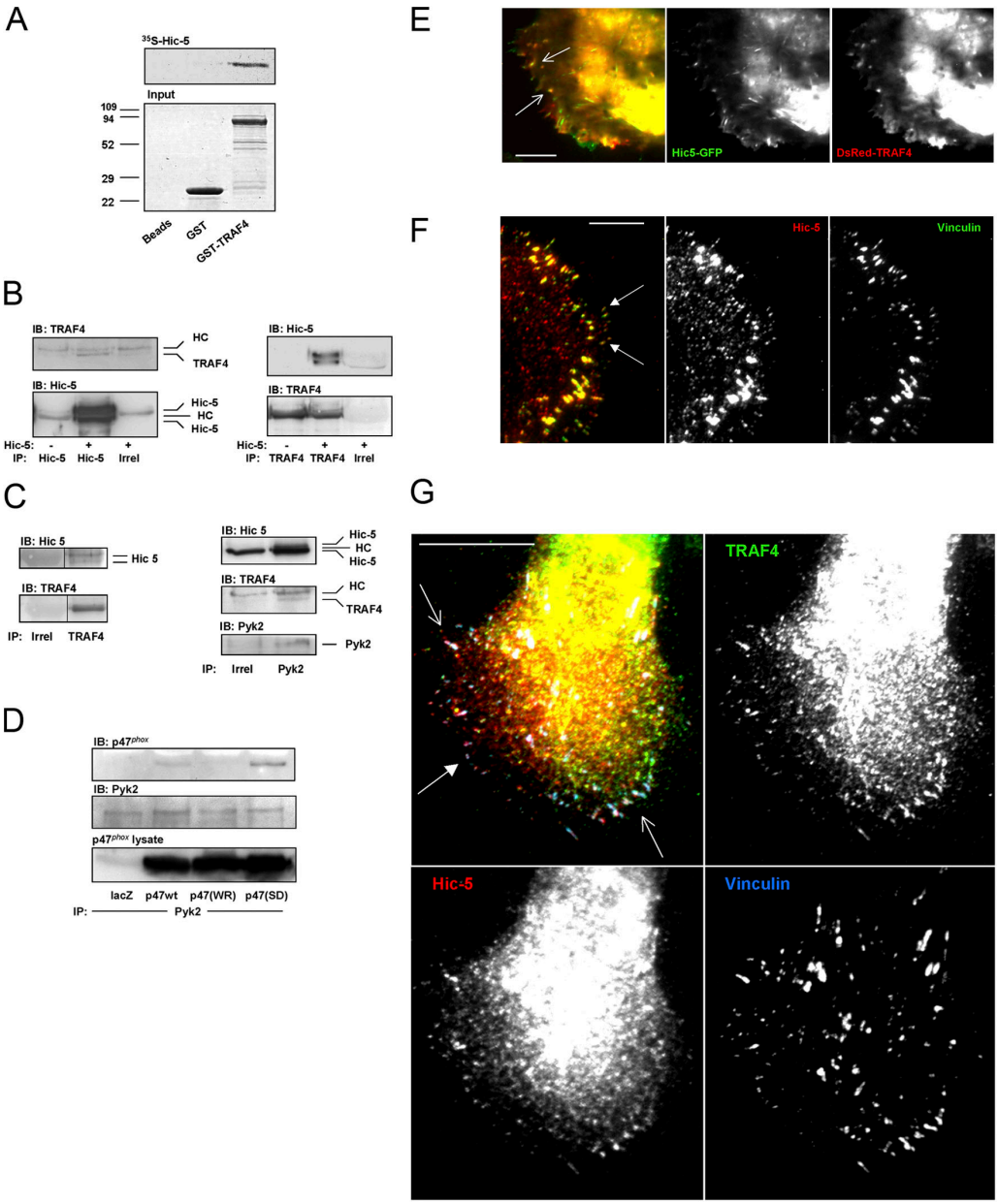

Figure 3. **TRAF4 associates with Hic-5.** (A) In vitro–translated full-length Hic-5 was specifically pulled down by GST-TRAF4, not by GST or beads alone. Top panel is an autoradiogram of captured ^{35}S-methionine–Hic-5; bottom panel is Coomassie stain of GST fusion input. (B) Phoenix-293 cells were transfected with TRAF4 with or without Hic-5 and immunoprecipitated with antibodies against Hic-5 (left), TRAF4 (right), or irrelevant antibodies. Immunoblots were sequentially probed for Hic-5 and TRAF4. Hic-5 appears as a doublet straddling the Ig heavy chain (HC). (C) Lysate from untransfected human lung microvascular endothelial cells was immunoprecipitated with antibodies for TRAF4 or Pyk2 and immunoblotted as shown. Endogenous Hic-5 coprecipitated with TRAF4 and both TRAF4 and Hic-5 coprecipitated with Pyk2. (D) HUVEC were infected with adenoviruses harboring *lacZ*, p47^{phox}(wt), p47(W193R), or p47(S303D,S304D,S328D) (MOI = 100:1). 24 h later, lysate was immunoprecipitated for Pyk2 and immunoblotted for p47^{phox} and Pyk2. Bottom panel shows total p47^{phox}. (E) Partial colocalization of Hic5-GFP and DsRed-TRAF4 at focal structures within the membrane edge (arrows) is seen. (F) Immunofluorescent image showing the presence of endogenous Hic-5 (AlexaFluor633) in small- to medium-sized vinculin (AlexaFluor555) structures at the edge of a protrusion (arrows). (G) Immunofluorescent stain showing the simultaneous appearance of TRAF4 (AlexaFluor488), Hic-5 (AlexaFluor633), and vinculin (AlexaFluor555) in small (closed head arrow) to medium (open head arrow)-sized complexes at the periphery of a lamella. E–G are TIRF microscopy images. Bars (E and F), 10 μm; (G) 20 μm.

TRAF4 or Hic-5 diminished HUVEC migration across fibronectin-coated filters in response to a VEGF gradient (Fig. 4 A). Furthermore, the superoxide dismutase mimetic MnTMPyP also inhibited endothelial cell migration, which is consistent with a role for oxidants in migration. Next, to determine relevant binding domains, truncations of each protein were expressed in vivo to preserve zinc finger structures. COOH-terminal truncations of Hic-5, which resulted in serial loss of the four COOH-terminal LIM domains and three LD motifs, revealed that only full-length Hic-5 coprecipitated with TRAF4 (Fig. 4 B), indicating that the COOH-terminal LIM domain 4 (residues 388–444) was necessary for TRAF4 binding. In addition, the Hic-5 LIM

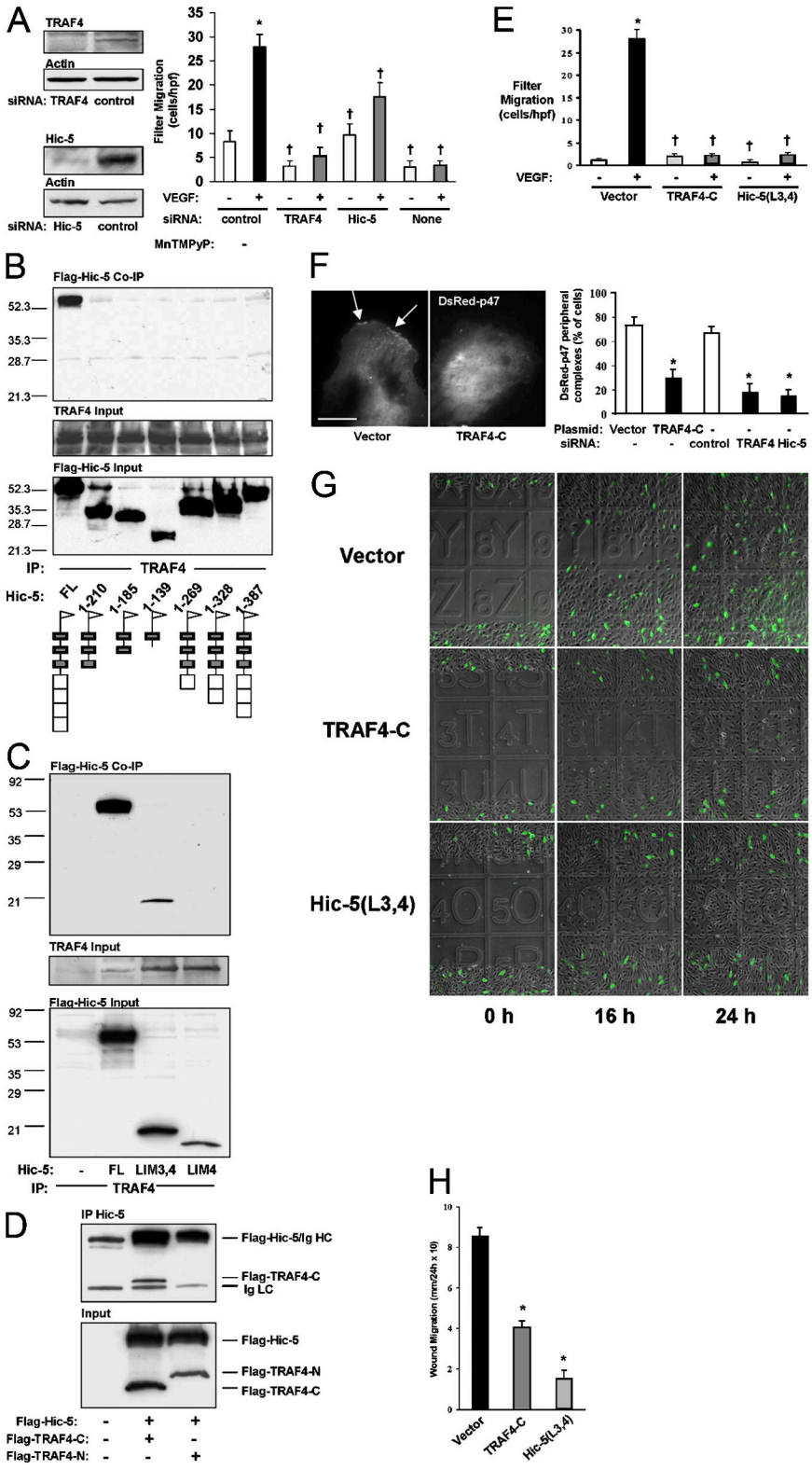

Figure 4. **TRAF4–Hic-5 interactions affect endothelial cell migration.** (A) HUVEC were transfected with siRNA against either TRAF4 or Hic-5, and migration across filters in response to a VEGF gradient was measured. Immunoblots show protein levels 48 h after transfection. Control siRNA was against luciferase. 100 μM MnTMPyP was present only during the 16-h migration period. Knockdown of Hic-5 or TRAF4 or antioxidant treatment decreased VEGF-induced migration of HUVEC. hpf, high-powered field. (B) Phoenix-293 cells were cotransfected with full-length TRAF4 and Flag-tagged Hic-5 truncations as indicated. Immunoblots of lysates before TRAF4 immunoprecipitation are shown as input. Cartoon below diagrams Hic-5 truncations showing NH_2-terminal Flag tag, three LD motifs (shaded), and four COOH-terminal LIM domains (open). Only full-length Flag–Hic-5 containing LIM 4 coprecipitated with TRAF4 (first lane). (C) Phoenix-293 cells were cotransfected with full-length TRAF4 and full-length Flag–Hic-5 (FL), Flag–Hic-5(329–444) (LIM3,4), or Flag–Hic-5(388–444) (LIM4). Lysates before TRAF4 immunoprecipitation were immunoblotted for Hic-5 and reprobed for TRAF4 to show input. Top panel shows coprecipitation of full-length Flag–Hic-5 and Flag–Hic-5(329–444) but not Flag–Hic-5(388–444) with TRAF4. (D) Phoenix-293 cells were cotransfected with full-length Flag–Hic-5 and either Flag-TRAF4(1–260) (TRAF4-N) or Flag-TRAF4(261–470) (TRAF4-C). Lysate was immunoblotted with anti-Flag (bottom) to show Hic-5 and TRAF4 inputs simultaneously. After immunoprecipitation with anti–Hic-5, blots were probed with anti-Flag to demonstrate the recovery of Flag–TRAF4-C but not Flag–TRAF4-N. Ig heavy and light chains (HC and LC) are shown. (E) HUVEC were cotransfected with pEGFP and empty vector (pCIN), TRAF4-C, or Hic-5(LIM3,4). GFP-expressing cells migrating across 8-μm pore filters in response to a VEGF gradient is shown. Migration in response to VEGF was blocked by the coexpression of either TRAF4-C or Hic-5(LIM3,4). (A and E) *, $P < 0.05$ compared with no VEGF control; †, $P < 0.05$ compared with VEGF control. (F) Discrete DsRed-p47 dotlike structures characteristically appeared at the edges of lamellar protrusions (arrows). Bar, 20 μm. Cotransfection of HUVEC with TRAF4-C or knockdown of endogenous TRAF4 or Hic-5 decreased the number of cells (*, $P < 0.05$) with such DsRed-p47 structures. (G) HUVEC were cotransfected as in D and plated on fibronectin-coated etched coverslips. Phase-contrast and epifluorescent (green) images were obtained immediately after wounding and at 16 and 24 h after wounding. (H) Histogram represents mean speed of GFP-expressing cells migrating into the wound. Entry of GFP-expressing cells into the wound was decreased by the coexpression of TRAF4-C or Hic-5(LIM3,4). Non–GFP-expressing cells migrated into wounds at comparable speeds. Error bars represent SEM. *, $P < 0.05$ compared with vector alone.

domain 4 in isolation did not coprecipitate with TRAF4, whereas the tandem LIM domains 3 and 4 (L3,4) did (Fig. 4 C). Thus, LIM domains 3 and 4 are each necessary but insufficient for TRAF4 binding. Conversely, full-length Hic-5 coprecipitated the COOH-terminal TRAF domain of TRAF4 (TRAF4-C) but not the NH_2-terminal remainder containing the ring and zinc fingers (Fig. 4 D). Thus Hic-5(L3,4) binds the COOH terminus of TRAF4.

Truncations comprising these two binding domains were then used to disrupt interactions between native proteins. Ectopic expression of either Hic-5(L3,4) or TRAF4-C, marked by cotransfection with GFP, abrogated VEGF-induced migration

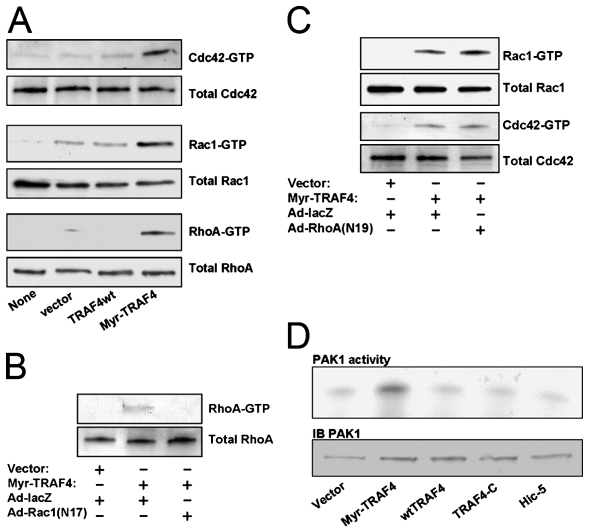

Figure 5. **Myr-TRAF4 activates Rho family GTPases and PAK1.** (A) HUVECs were transfected with empty vector, native TRAF4 (wt), or Myr-TRAF4. After 24 h, cells were lysed, and GTP-loaded Rho proteins were captured with GST-CRIB or GST–Rho-binding domain. Immunoblots for Cdc42, Rac1, and RhoA are shown in lysates and after capture. (B and C) HUVECs were transfected with the indicated vectors, infected with Ad-*lacZ*, Ad-RhoA(N19), or Ad-Rac1(N17) (MOI = 100:1), and RhoA, Rac1, and Cdc42 activity were assessed. Myr-TRAF4 activated Cdc42 and Rac1 upstream of RhoA. (D) HUVECs were transfected with the indicated plasmids and assessed for PAK1 activity by immunoprecipitation kinase. Phosphorylation of myelin basic protein (top) and immunoblot for captured PAK1 (bottom) are shown. Myr-TRAF4 but not wtTRAF4 activated PAK1.

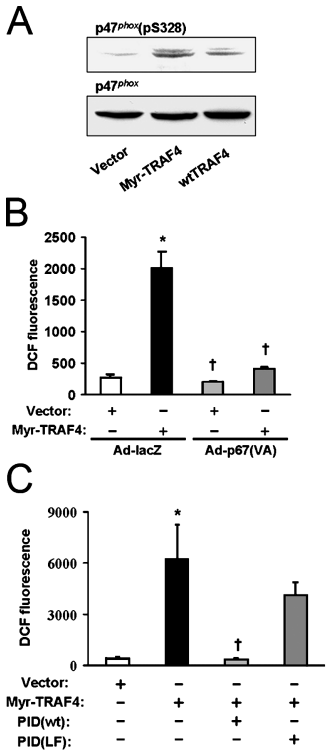

Figure 6. **Myr-TRAF4 activates the NADPH oxidase through PAK1.** (A) Phoenix-293 cells overexpressing wt-p47^{phox} were transfected with the indicated plasmids. Whole cell lysates were immunoblotted for p47^{phox} (pS328) and reprobed for total p47^{phox}, demonstrating phosphorylation of p47(S328) by Myr-TRAF4. (B) HUVECs were cotransfected with DsRed and one of the indicated plasmids and were infected with Ad-*lacZ* or Ad-p67(V204A). DCF fluorescence of adherent DsRed-expressing cells was quantified by image analysis as described in Oxidant production. Myr-TRAF4–induced oxidant production was blocked by p67(V204A). (C) HUVECs were cotransfected with DsRed and the indicated plasmids, and oxidant production of DsRed-expressing cells was measured without manipulation. The PAK inhibitory domain (PID(wt)) but not its nonbinding mutant (PID(LF)) decreased Myr-TRAF4–induced oxidant production. (B and C) *, $P < 0.05$ compared with control; †, $P < 0.05$ compared with Myr-TRAF4 alone. Error bars represent SEM.

(Fig. 4 E). Consistent with the ability of TRAF4 to direct p47^{phox} to focal complexes, the expression of TRAF4-C, which also contains the p47^{phox}-binding site, or the knockdown of either TRAF4 or Hic-5 caused the delocalization of DsRed-p47 from its sites of peripheral focal accumulation (Fig. 4 F). In addition, GFP-cotransfected cells expressing Hic-5(L3,4) or TRAF4-C failed to participate in sheet migration into monolayer wounds despite wound closure by nontransfected cells (Fig. 4, G and H), providing further evidence for a functional TRAF4–Hic-5 complex.

Myr-TRAF4 activates Rho GTPases, PAK1, and the NADPH oxidase

An active mutant of TRAF4 was created through NH_2-terminal fusion with the c-Src myristoylation motif (Myr-TRAF4). Myr-TRAF4 was isolated from detergent-resistant low density membrane fractions, which is consistent with raft localization, and also from the insoluble pellet fraction, which is consistent with cytoskeletal association (Fig. S3, available at http://www.jcb.org/cgi/content/full/jcb.200507004/DC1). Surprisingly, both endogenous TRAF4 and overexpressed native TRAF4 also quantitatively partitioned with raft fractions, although cytoskeletal association was weak. Raft localization of TRAF4 is consistent with the site of integrin activation upon matrix attachment (Lacalle et al., 2002; Labrecque et al., 2003).

The Rho family of small GTPases associate avidly with raft domains upon activation (del Pozo et al., 2004) and control focal complex dynamics, migration, and NADPH oxidase activation. Using GST fusions of the PAK1 Cdc42–Rac1 interaction binding (CRIB) domain or the rhotekin Rho-binding domain in pull-down assays, we found that Myr-TRAF4 stimulated GTP loading of Cdc42, Rac1, and RhoA (Fig. 5 A). Furthermore, Rac1(N17) diminished Myr-TRAF4–induced RhoA activation, whereas RhoA(N19) had no effect on Rac1 or Cdc42 activation (Fig. 5, B and C). Thus, TRAF4 activates Cdc42 and Rac1 upstream of RhoA, which is consistent with the sequence of Rho GTPase activation during spontaneous focal contact formation after matrix attachment (Nobes and Hall, 1995). Confirming the activation of Rho GTPases in vivo, Myr-TRAF4 constitutively activated the Cdc42 and Rac1 effector PAK1 (Fig. 5 D). In some cells (presumably high transgene expressors), actin cytoskeletal collapse was noted (Fig. S4, available at http://www.jcb.org/cgi/content/full/jcb.200507004/DC1), which is a morphology resulting from the expression of active PAK1 mutants (Manser et al., 1997) or agonist-dependent PAK1 activation (Wu et al., 2004). Indeed, adenoviral delivery of kinase-dead PAK1(K298A) completely suppressed Myr-TRAF4–induced cytoskeletal remodeling (Fig. S4).

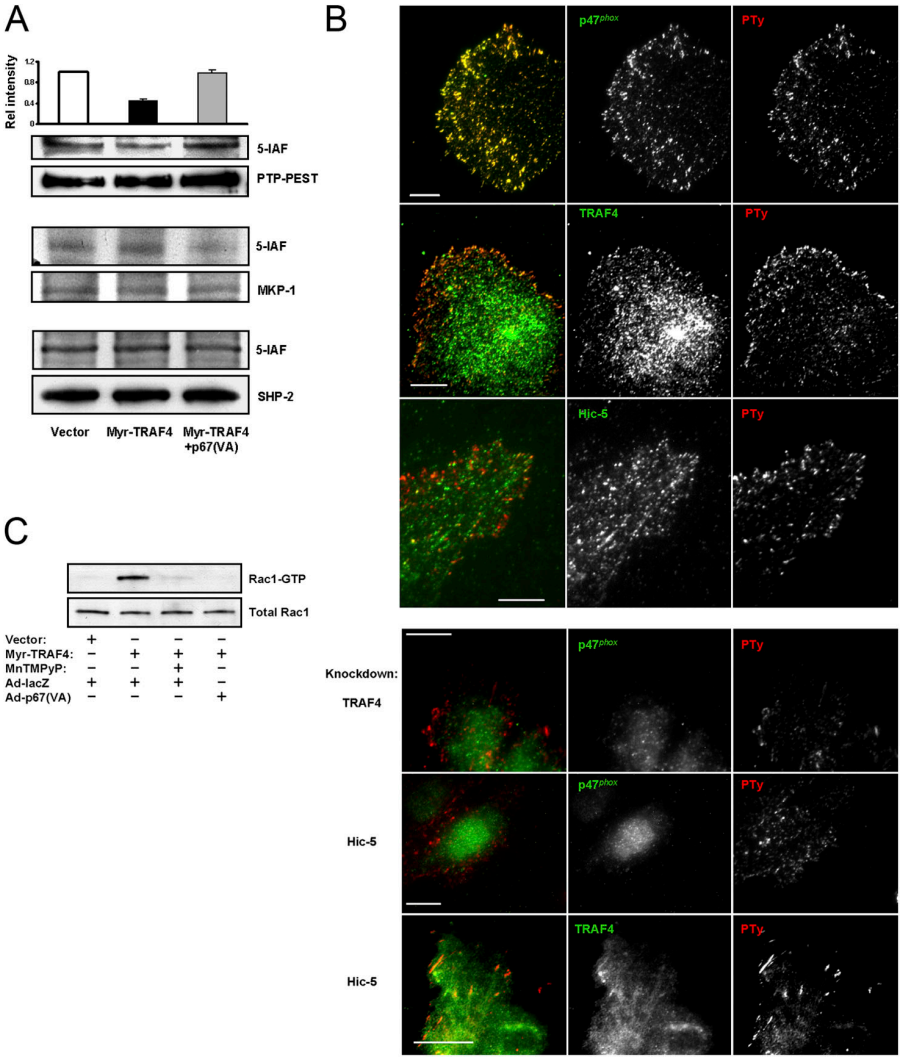

Figure 7. **Myr-TRAF4 oxidatively modifies the focal contact phosphatase PTP-PEST through the NADPH oxidase.** (A) Phoenix-293 cells were transfected with either empty vector or Myr-TRAF4. In top panels, cells were cotransfected with Flag–PTP-PEST. p67(V204A) was adenovirally transduced. Lysates were labeled with 5-IAF, and the indicated PTPs were immunoprecipitated and immunoblotted for fluorescein to detect 5-IAF labeling and for the respective PTPs to assess capture. Myr-TRAF4 decreased 5-IAF labeling of PTP-PEST, indicating oxidative modification of the active site cysteine. 5-IAF labeling of MKP-1 and SHP-2 was unaffected. Error bars represent SEM. (B) Immunofluorescent images were obtained with TIRF microscopy showing colocalization of $p47^{phox}$, TRAF4, and Hic-5 (AlexaFluor488 or 633) with phosphotyrosinylated proteins (AlexaFluor555) within peripheral dots at the edges of protrusions. In bottom panels, endogenous TRAF or Hic-5 were knocked down in HUVECs as indicated. Bars, 10 μm. (C) HUVECs were transfected with the indicated plasmids and infected with the indicated Ad viruses. 200 μM MnTMPyP was present for 3 h before lysis. Rac1 GTP loading was assessed by binding to GST-CRIB. Both MnTMPyP and p67(V204A) blocked Myr-TRAF4–induced Rac1 activation.

PAK1 not only targets focal complexes (Manser et al., 1998; Zhao et al., 2000) and becomes active within membrane rafts (Krautkramer et al., 2004), but it has been shown to act upstream of the NADPH oxidase in endothelial cells (Wu et al., 2003, 2004). An early event in oxidase activation is the serine phosphorylation of $p47^{phox}$, which unmasks binding domains (Faust et al., 1995). To assess NADPH oxidase activation, we developed antisera against $p47^{phox}$ phosphorylated on S328, a key phosphorylation site (Ago et al., 1999), and found that the expression of Myr-TRAF4 in Phoenix-293 cells increased $p47^{phox}$ S328 phosphorylation (Fig. 6 A). Accordingly, Myr-TRAF4 increased oxidant production in HUVECs, and this oxidant production was decreased by the NADPH oxidase–specific transdominant antagonist p67(V204A) (Fig. 6 B). Furthermore, oxidant production was completely blocked by the PAK inhibitory domain (PID), which binds and inhibits the PAK kinase domain (Fig. 6 C). In contrast, the PID harboring an equivalent of the PAK1(L107F) mutant, which was predicted to disrupt this interaction (Frost et al., 1998), had no significant effect. Thus, Myr-TRAF4 activates Rac1 and increases oxidant production through PAK1-dependent NADPH oxidase activation.

Myr-TRAF4 oxidatively modifies PTP-PEST

A prominent and perhaps central mechanism by which oxidants exert their effects on signaling pathways is through oxidative modification of the conserved catalytic cysteine of protein tyrosine phosphatases, rendering them inactive (Meng et al., 2002). PTP-PEST represents a potential oxidant target because it binds Hic-5, targets nascent focal contacts, blocks integrin-dependent Rac1 activation, and modulates cell migration (Angers-Loustau et al., 1999; Nishiya et al., 1999; Sastry et al., 2002). Therefore, we examined oxidative inactivation of PTP-PEST by assessing its covalent labeling with 5′-iodoacetamidofluorescein (5-IAF), which is known to selectively react with the acidic catalytic cysteine thiol of active PTPs (Wu et al., 1998). We found that Myr-TRAF4 increased oxidative modification (decreased 5-IAF labeling) of the acidic cysteine of coexpressed PTP-PEST in Phoenix-293 cells (Fig. 7 A). The expression of p67(V204A) completely prevented this oxidative modification, which is consistent with the predominant effect of the NADPH oxidase on PTP-PEST.

To assess the specificity of this effect, we examined the effect of Myr-TRAF4 on two other PTPs. First, MAPK phos-

phatase (MKP-1) is also oxidant sensitive (Kamata et al., 2005) but largely cytosolic and, thus, is not expected to be targeted by TRAF4-directed oxidants. Indeed, Myr-TRAF4 had no effect on 5-IAF labeling of MKP-1 (Fig. 7 A). More interestingly, SHP-2 is also oxidant sensitive (Meng et al., 2002) and, in addition, controls integrin signaling (Lacalle et al., 2002). Unlike PTP-PEST, however, SHP-2 appears to govern insulin signaling and stable focal adhesion dynamics and does so through control of RhoA, not Rac1 (Manes et al., 1999; Inagaki et al., 2000; Kontaridis et al., 2004). Accordingly, we found that Myr-TRAF4 did not affect 5-IAF labeling of SHP-2, suggesting that the effects of TRAF4-linked oxidants are not generalized for all integrin structures and that they possess some degree of specificity for PTP-PEST. As a further demonstration that the TRAF4–oxidase complex facilitates tyrosine phosphorylation of integrin aggregates, we found using immunofluorescence that endogenous Hic-5, TRAF4, and p47^{phox} colocalized with tyrosine-phosphorylated structures at the edge of membrane protrusions (Fig. 7 B). These findings are consistent with the accumulation of tyrosine-phosphorylated proteins within focal complexes (Allen et al., 1997). Knockdown of either TRAF4 or Hic-5 qualitatively decreased but did not abolish focal contact tyrosine phosphorylation and decreased p47^{phox} association with focal contacts. As expected, the knockdown of Hic-5 also decreased the targeting of TRAF4 to tyrosine-phosphorylated structures (Fig. 7 B).

Although our data indicate that TRAF4 activates a Rac1/PAK1/NADPH oxidase cascade, leading to oxidative inactivation of PTP-PEST, the latter phosphatase in its active form has been shown to decrease attachment-dependent Rac1 activation, possibly feeding back upstream in this cascade (Sastry et al., 2002). Were this the case, Rac1-dependent oxidant production would be expected to further increase Rac1 activity, thereby engaging in a positive feedback cycle. To test this hypothesis, we examined the effect of the NADPH oxidase on its upstream activator, Rac1. Indeed, both MnTMPyP and p67(V204A) completely suppressed Myr-TRAF4–induced Rac1 GTP loading (Fig. 7 D), placing the oxidase both upstream and downstream of TRAF4-dependent Rac1 activation.

TRAF4-dependent membrane ruffling proceeds through Rac1, PAK1, and the NADPH oxidase

The expression of Myr-TRAF4 by endothelial cells caused dramatic membrane ruffling on multiple edges with a concentration of DsRed-p47 within ruffles, suggesting diffuse constitutive activation of Rac1 and PAK1 and high focal complex turnover (Fig. 8 A). Extensive lamella formation was occasionally seen in conjunction with ruffling (not depicted). As expected, Rac1(N17) diminished ruffling to basal levels (Fig. 8 B). In addition, kinase-inactive PAK1(K298A) and wild-type PID (but not the inactive PID[LF] mutant peptide) also blocked Myr-TRAF4–induced ruffling (Fig. 8 B). Finally, both MnTMPyP and p67(V204A) reduced Myr-TRAF4–induced ruffling to basal levels (Fig. 8 C). Thus, by morphological as well biochemical criteria, Rac1, PAK1, and the NADPH oxidase act downstream of TRAF4.

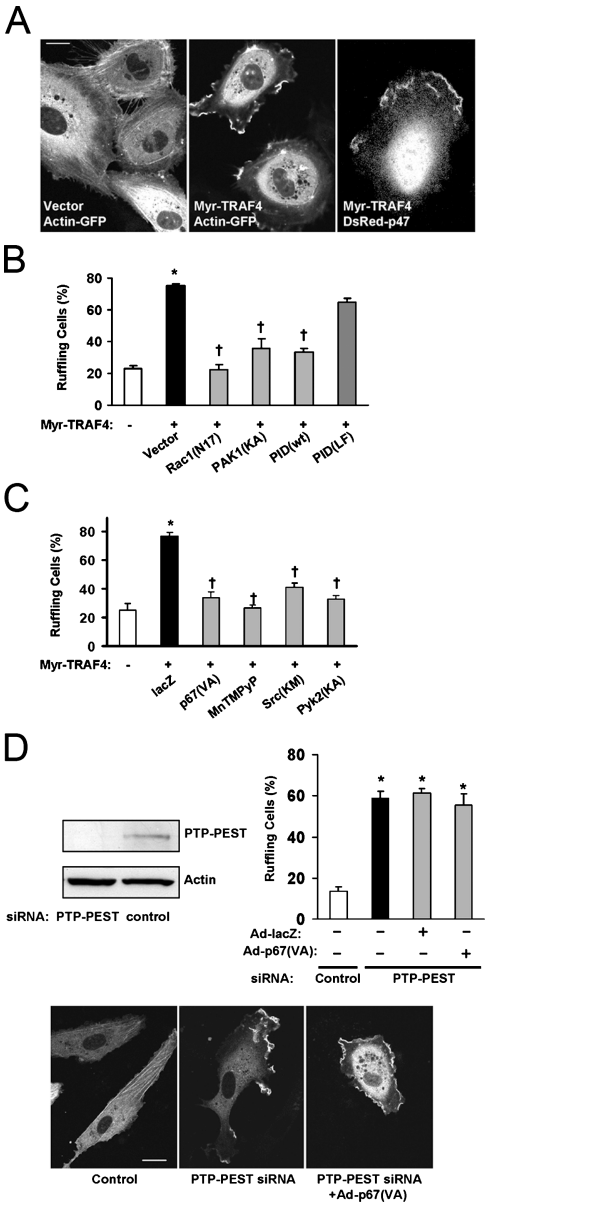

Figure 8. **Myr-TRAF4 induces marked membrane ruffling through Rac1, PAK1, and the NADPH oxidase.** (A) HUVECs were cotransfected with either empty vector or Myr-TRAF4 and either actin-GFP or DsRed-p47. Myr-TRAF4–induced ruffling is seen on multiple edges of cotransfected cells (middle). Ruffles contained DsRed-p47 (right). (B and C) HUVECs were cotransfected with actin-GFP and either empty vector (first bar) or Myr-TRAF4 and additionally with one of the indicated plasmids. PAK1(K298A) and p67(V204A) were expressed via adenoviral transduction. 100 μM MnTMPyP was added for 1 h. Inhibition of PAK1, the NADPH oxidase, Pyk2, or Src decreased the percentage of cells ruffling in response to Myr-TRAF4. *, $P < 0.05$ compared with vector control; †, $P < 0.05$ compared with Myr-TRAF4 alone. (D) HUVECs were transfected with siRNA against PTP-PEST. Immunoblot shows protein levels after 48 h. PTP-PEST knockdown increased the percentage of ruffling cells. *, $P < 0.05$ compared with control siRNA. Expression of p67(V204A) had no effect on the ruffling rate in PTP-PEST knockdown cells. Examples are shown below. Error bars represent SEM. Bars, 20 μm.

If PTP-PEST were an essential target in TRAF4-directed oxidant signaling, a specific decrease in PTP-PEST activity independent of TRAF4 should similarly be manifested as an increase in ruffling. Indeed, siRNA-mediated knockdown of

PTP-PEST promoted robust membrane ruffling in the absence of Myr-TRAF4 (Fig. 8 D). This effect is similar to the enhancement in ruffling elicited by the expression of the catalytically inactive PTP-PEST(C321S) (Sastry et al., 2002), which, in theory, should behave like an oxidatively inactivated phosphatase. The expression of p67(V204A) had no effect on this ruffling, which is consistent with the effects of the NADPH oxidase upstream of PTP-PEST inactivation. Although it is not clear that all of the effects of TRAF4-directed oxidant production funnel through PTP-PEST inactivation, the depletion of active PTP-PEST appears to be at least sufficient to mediate ruffling.

PTP-PEST antagonizes the effects of the tyrosine kinase Pyk2 (Lyons et al., 2001). The latter protein, which is associated with the p47^{phox}–TRAF4–Hic-5 complex (Fig. 3 C), acts as a scaffold for another focal complex tyrosine kinase, Src, and facilitates Src activation (Park et al., 2004). Src, in turn, mediates focal complex turnover much like active PAK1 (Manser et al., 1997; Zhao et al., 2000; Webb et al., 2004). Accordingly, we found that kinase-dead mutants of both Pyk2 and Src also caused Myr-TRAF4–transfected endothelial cells to lose membrane ruffles and become quiescent (Fig. 8 C), which is consistent with the focusing of TRAF4's effects on focal complex tyrosine phosphorylation events related to PTP-PEST.

Finally, as many of the proteins implicated in TRAF4 signaling (including TRAF4 itself, Rac1, PAK1, the NADPH oxidase cytochrome subunits, integrins, and Src) congregate within membrane rafts, it was not surprising to find that the disruption of raft structure with either filipin (not depicted) or methyl-β cyclodextrin (Fig. S5, available at http://www.jcb.org/cgi/content/full/jcb.200507004/DC1) effectively diminished Myr-TRAF4–induced ruffling and lamellipodium formation. Although not specific for the TRAF4 complex, these data support the concept that TRAF4 operates within an expected microdomain to participate in Rac1-dependent integrin signaling.

Discussion

By sequence homology and domain organization, human TRAF4 is closer to the canonical *Drosophila melanogaster* orthologue dTRAF1 than to all other mammalian TRAF members, suggesting an early evolutionary and functional bifurcation of TRAF4 from other human TRAFs. Indeed, no immunological defects have been identified to date in mice lacking TRAF4. Instead, TRAF4 deficiency leads to defective ontogenic migration, resulting in incomplete neural tube and branchial arch closure (Regnier et al., 2002). Accordingly, TRAF4 was originally cloned based on its differential expression in metastatic breast cancer tissues (Tomasetto et al., 1995), suggesting a link between TRAF4 and the epithelial–mesenchymal transition. In endothelial cells, TRAF4 controls NADPH oxidase–dependent activation of JNK (a MAPK involved in migration) through disparate agonists invoked in angiogenesis (Xu et al., 2002). Similarly, the fly orthologue dTRAF1 was originally identified by its involvement in the Misshapen/JNK cassette that controls cell migration during fly embryogenic dorsal closure downstream from Rho/Rac (Liu et al., 1999; Lu and Settleman, 1999). The loss of dTRAF1 also results in the failure of JNK activation during metamorphosis with impaired dorsal thoracic closure (Cha et al., 2003). Despite these inferences, however, TRAF4 has not previously been placed within a pathway that is relevant to cell migration.

Our data suggest that during cell migration, TRAF4 may tether p47^{phox} to nascent lamellar focal complexes to direct oxidant production to these structures and bias the local environment toward tyrosine phosphorylation events and Rho GTPase activation. We provide microscopic, biochemical, and functional evidence for such targeting. First, we found that both chromophore fusions of TRAF4 and p47^{phox} as well as the endogenous proteins are targeted to leading edge focal complexes, which are integrin-associated structures concentrated with tyrosine-phosphorylated proteins. This physical targeting of an NADPH oxidase subunit to such structures is consistent with the influence of integrin ligation on oxidase activation; for instance, either the detachment or reattachment of cells to the matrix induces NADPH oxidase–dependent oxidant production (Kheradmand et al., 1998; Chiarugi et al., 2003). The appearance of TRAF4 in membrane rafts is also consistent with its functional interaction with integrin structures and the NADPH oxidase. Matrix attachment, for instance, directs β_1 and β_3 integrins into raft domains (Lacalle et al., 2002; Labrecque et al., 2003); in addition, the NADPH oxidase membrane–associated cytochrome b_{558} (gp91^{phox} and p22^{phox}), like TRAF4, is constitutively associated with lipid rafts (Vilhardt and Van Deurs, 2004). The further appearance of Src, Rac1, and RhoA in rafts after integrin ligation also suggests the importance of rafts as organizing structures involved in focal complex dynamics.

Second, we found evidence that a functional complex is formed along with the focal contact protein Hic-5. TRAF4 binds Hic-5 and forms a complex with the focal adhesion kinase Pyk2, a redox-sensitive kinase previously shown to mediate VEGF-induced endothelial cell migration (Avraham et al., 2003). Accordingly, knockdown of either TRAF4, Hic-5, or binding truncations of either protein disrupt VEGF-mediated chemotaxis and sheet migration into wounds. The association of TRAF4 with Hic-5 suggests a mechanism of specifying oxidase activation to integrin complexes and potentially places such a complex in proximity to other oxidant-related, Hic-5–associated proteins. These include PAK1, which associates with Hic-5 through paxillin-kinase linker (Turner et al., 1999) and both associates with p47^{phox} and acts upstream of its phosphorylation (Wu et al., 2003, 2004); Pyk2, which binds to the NH_2 terminus of Hic-5 (Matsuya et al., 1998) and requires endogenous oxidants for integrin-dependent mechanosensory activation (Tai et al., 2002); and Src, which binds Pyk2 (Matsuya et al., 1998; Park et al., 2004), phosphorylates Hic-5 (Matsuya et al., 1998; Ishino et al., 2000), and becomes active upon integrin ligation via oxidant production (Chiarugi et al., 2003). Besides acting up or downstream of endogenous oxidants, all three of these kinases increase focal complex turnover and mediate ruffle formation as well as cell migration (Manser et al., 1997; Kiosses et al., 1999; Timpson et al., 2001; Okigaki et al., 2003; Webb et al., 2004).

Third, we found that a myristoylated form of TRAF4 activates Rho GTPases and the effector kinase PAK1, increases

p47^{phox} phosphorylation and oxidant production, and causes intense membrane ruffling, which is a morphologic correlate of Rac1 hyperactivation. Our data further suggest that oxidants facilitate focal complex signaling through the targeted inactivation of PTP-PEST. This phosphatase binds Hic-5 and translocates to nascent focal complexlike structures (Angers-Loustau et al., 1999; Nishiya et al., 1999; Sastry et al., 2002), where it can gainsay both Pyk2 and Src function (Angers-Loustau et al., 1999; Lyons et al., 2001). Notably, active PTP-PEST decreases Rac1 activity and membrane ruffling and is thought to participate in focal contact turnover (Angers-Loustau et al., 1999; Sastry et al., 2002; Cousin and Alfandari, 2004). Consistent with the combined observations that PTP-PEST may act both up and downstream of Rac1, we found that the NADPH oxidase may act similarly, thus participating in a possible positive feedback loop. Such loops are thought to be critical in sensing and amplifying shallow chemoattractant gradients and fully polarizing the motile cell (for review see Ridley et al., 2003). Interestingly, these loops involve PI3K, PAK1, and Rho GTPases such as Rac1, which are all capable of acting upstream of the NADPH oxidase and are all rapidly mobilized to the leading edge.

Materials and methods

Plasmid and adenoviral derivation

Full-length human TRAF4 (Xu et al., 2002) was PCR amplified and subcloned into pDsRed2-N1 or pEGFP-N3 (CLONTECH Laboratories, Inc.) to create DsRed-TRAF4 and TRAF4-GFP. TRAF4(1–260) was amplified and subcloned into pCINF to create TRAF4-N. Annealed oligonucleotides encoding the NH_2-terminal c-Src myristoylation sequence (MGSSKSKPKDPSQRRR) were ligated into pCI-neo, and TRAF4 was then inserted in frame to form Myr-TRAF4. After the creation of BamHI and EcoRI sites, TRAF4 was subcloned into pGEX-2TK. Full-length Hic-5 was PCR amplified from a HUVEC cDNA library (Xu et al., 2002), ligated into pCINF in frame with an NH_2-terminal Flag tag, and subcloned into pEGFP-N3 to form Hic5-GFP. Serial COOH-terminal truncations of Hic-5 ending with residues 139, 185, 210, 269, 328, and 387 were generated by PCR from pCINF-Hic5. Hic-5(329–445) and (388–444) corresponding to the LIM-3,4 and LIM-4 domains were PCR amplified and inserted into pCINF. PTP-PEST was PCR amplified from a HUVEC library and subcloned into pCINF. The PAK1 autoinhibitory domain (residues 83–149 of rat PAK1) was subcloned into pCINF. The PAK1(L107F) mutant was obtained from Melanie Cobb (University of Texas Southwestern, Dallas, TX), and the corresponding mutant PID was subcloned into pCINF. TRAF4(261–470), p47-GFP, DsRed-p47, pGBKT7-TRAF4, and pCI-TRAF4 were previously described (Gu et al., 2002; Xu et al., 2002; Wu et al., 2003). All constructs were sequenced for verification. Zyxin-GFP, DsRed-zyxin, Src(K295M), and Pyk2(K457A) were gifts from Derek Toomre (Yale University, New Haven, CT), Anna Huttenlocher (University of Wisconsin, Madison, WI), Serge Roche (Centre de Recherches de Biochimie Macromoléculaire, Montpellier, France), and Shalom Avraham (Harvard University, Boston, MA), respectively. Adenoviruses harboring PAK1(K298A), p67^{phox}(V204A), and p47^{phox}(wt) (W193R) and (S303D,S304D,S328D) mutants were constructed as described previously (Xu et al., 2002; Wu et al., 2003, 2004). Adenoviruses containing Myc-Rac1(N17) and RhoA(N19) were gifts from Kaikobad Irani (Johns Hopkins University, Baltimore, MD) and Christopher Chen (University of Pennsylvania, Philadelphia, PA), respectively (Ozaki et al., 2000; McBeath et al., 2004).

Microscopy

HUVECs were grown in EGM-2 media (Clonetics), electroporated 6–7 h after release from thymidine-induced cell cycle arrest, and plated on fibronectin-coated chambered coverslips (Lab-Tek). Because endothelial edge ruffles do not readily withstand fixation/permeabilization, cells were examined live with sequential acquisition of red and green channels. Confocal microscopy was performed using a LSM 410 laser scanning system (Axiovert S100TV; Carl Zeiss MicroImaging, Inc.). Images were acquired with either a 63×/1.2 or a 100×/1.3 objective using LSM software (Carl Zeiss MicroImaging, Inc.). Ruffling was quantified in actin-GFP–cotransfected cells by examining all cells in at least four high power fields per chamber in at least four chambers. TIRF microscopy was performed on live cells using a fluorescent inverted microscope system (TE2000-U; Nikon). Images were acquired at 37°C with a 60×/1.45 oil immersion objective (Nikon) using Metamorph software (Molecular Devices).

Immunofluorescence

HUVEC plated on fibronectin-coated chambered coverslips were washed, fixed with 2% HCHO, and permeabilized with 0.2% Triton X-100. After subsequent washing, cells were blocked at 25°C for 30 min with either 10% normal goat serum or 5% BSA. Primary antibodies used were Hic-5 (1:50; Santa Cruz Biotechnology, Inc.), TRAF4 (1:50; Santa Cruz Biotechnology, Inc.), p47^{phox} (1:50; Santa Cruz Biotechnology, Inc.), vinculin (1:100; clone Vin-11-5; Sigma-Aldrich), and phosphotyrosine (1:200; clone PT-66; Sigma-Aldrich); these antibodies were incubated with cells at 25°C for 1 h in either 5% goat serum or 2% BSA. Corresponding secondary antibodies conjugated to AlexaFluor488, 555, or 633 were obtained from Invitrogen. Cells were stained with each secondary antibody separately with extensive washing in between. Cells were observed with TIRF microscopy as described above using 488-, 543-, or 633-nm excitation lines. Corresponding controls without primary antibodies were confirmed to be negative, and no bleed-through to other channels was observed with any of the chromophores.

Yeast two-hybrid screening

A HUVEC library was previously constructed in lambda phage HybriZAP 2.1 XR (Xu et al., 2002), and the library was dropped out in the yeast shuttle vector pAD-GAL4-2.1 by mass excision. *Saccharomyces cerevisiae* AH109 (CLONTECH Laboratories, Inc.) were sequentially transformed with the bait vector pGBKT7-TRAF4 and with the endothelial library using lithium acetate. Candidate prey were identified with adenine and histidine auxotrophic selection and *lacZ* expression. Single yeast clones were retested for auxotrophy and *lacZ* expression, and library plasmids were passaged through *Escherichia coli* and confirmed with standard yeast mating techniques. Interactions were assessed using yeast mating techniques, with the assessment of *lacZ* expression by diploids. In vitro pull down was performed as previously described (Xu et al., 2002).

Coimmunoprecipitation

Phoenix-293 cells electroporated with indicated vectors were extracted in lysis buffer (20 mM Tris, pH 7.5, 150 mM NaCl, 1 mM EDTA, 1 mM EGTA, 1% Triton X-100, 2.5 mM Na pyrophosphate, 1 mM β-glycerophosphate, 1 mM Na_3VO_4, 1 μg/ml leupeptin, and 1 mM PMSF) for 30 min on ice, sonicated for 5 s, and centrifuged at 10,000 *g* for 20 min at 4°C. Immunoprecipitation was then performed using protein A or protein G–agarose (GE Healthcare) conjugates. Antibodies used are as follows: TRAF4 (Santa Cruz Biotechnology, Inc.), Flag (Sigma-Aldrich), Hic-5 and Pyk2 (BD Transduction), and p47^{phox} (Upstate Biotechnology and gift of Bernard Babior, Scripps Research Institute, La Jolla, CA). In some experiments, human lung microvascular endothelial cells or HUVECs (both from Clonetics) were used.

Protein knockdown

RNA corresponding to both strands of human Hic-5 (803–821), TRAF4 (175–193), and PTP-PEST (1584–1602; coding region numbering) tailed with dTdT were synthesized by Dharmacon. A sequence from firefly luciferase was used as a control siRNA in all experiments. 10 nM duplex siRNA was transfected into HUVEC using 30 μl TransIT-TKO (Mirus) per 100-mm dish. Protein expression was assessed, and experiments were initiated after 48 h.

Migration assays

The bottom of 24-well transwell filters (0.8 μm; Costar) was coated with fibronectin (Sigma-Aldrich). HUVECs were cotransfected with pEGFP (CLONTECH Laboratories, Inc.) and one of the indicated vectors. 24 h after transfection, cells were plated onto filters in growth factor–deficient EBM2 media (Clonetics) with 2% FBS. The bottom chamber contained the same media plus 100 ng/ml VEGF (PeproTech). Cells were allowed to migrate for 16 h, and then cells remaining on the top surface were removed with a cotton swab and GFP-positive cells were counted. After counting, cells were swabbed off the bottom surface, and the filters were reexamined to confirm the removal of remaining cells. Migration into wounds was examined by plating pEGFP-cotransfected HUVECs on fibronectin-coated etched coverslips (Bellco). At least five wounded fields per coverslip were analyzed on six coverslips per condition, and identical

fields were photographed under phase and epifluorescence at 0, 18, 24, and 48 h. Phase-contrast and GFP images were overlaid and analyzed using Metamorph software.

Raft fractionation

Detergent-insoluble low density fractions were isolated as described previously (Lee et al., 2002). Five 100-mm dishes per condition were pooled, washed twice with PBS, and resuspended in 1 ml MES-buffered saline (MBS; 25 mM MES, pH 6.5, 150 mM NaCl, and 5 mM EDTA) with 1% Triton X-100 and protease inhibitors. Cells were disrupted with 10 passes through a 25-gauge needle and diluted with 1 ml 80% sucrose in MBS. Lysate was overlaid with 2 ml of 30% and 1 ml of 5% sucrose in MBS and centrifuged at 200,000 *g* for 18 h at 4°C with a rotor (SW55Ti; Beckman Coulter). 0.4-ml fractions were removed from the top, acetone precipitated twice, washed in acetone, and resuspended in Laemmli buffer. Antibodies for caveolin-1, Rac1, TfR, and TRAF4 were obtained from Santa Cruz Biotechnology, Inc.

Rho family GTP loading

The human PAK1 CRIB domain (residues 51–135) was recovered by PCR from a HUVEC library and ligated into pGEX-2TK, and the Rho-binding domain of mouse rhotekin (residues 7–89) was recovered by RT-PCR from mouse endothelial cells and ligated into pGEX-2TK. GST fusion proteins were then produced in BL21-RP bacteria and captured on glutathione S-transferase–Sepharose beads (GE Healthcare). Active GTP-loaded Rho proteins from the 10,000-g supernatant of HUVEC lysate were pulled down by the respective fusions and immunoblotted with antisera for Rac1 (BD Transduction), Cdc42 (Santa Cruz Biotechnology, Inc.), or RhoA (Santa Cruz Biotechnology, Inc.).

PAK1 activity

PAK1 activation was assessed by an immunoprecipitation kinase assay (Wu et al., 2004). In brief, HUVECs were extracted in cold lysis buffer, sonicated briefly, centrifuged, and immunoprecipitated with rabbit anti-PAK1 (Santa Cruz Biotechnology, Inc.). The kinase reaction was performed using 5 μg myelin basic protein as a substrate in the presence of γ-[^{32}P]ATP at 30°C for 30 min. Two thirds of each sample was subjected to autoradiography, and one third was subjected to immunoblotting to assess the capture of PAK1.

p47^{phox} phosphorylation

Rabbit polyclonal antisera was raised by immunization with a keyhole limpet hemocyanin–conjugated peptide YRRN(pS)VRFLQQRR containing a phosphoserine corresponding to S328 of human p47^{phox}. The antisera specifically recognized p47^{phox} phosphorylated in vivo by phorbol ester stimulation. Phoenix-293 cells overexpressing p47^{phox} were transfected with pCIN, Myr-TRAF4, or TRAF4, and whole cell lysates were serially immunoblotted for p47^{phox}(pS328) and total p47^{phox} (Upstate Biotechnology).

Oxidant production

HUVECs were cotransfected with pDsRed-C2 and the test vectors, plated on fibronectin-coated slides, and subsequently infected with adenovirus (multiplicity of infection [MOI] = 100:1). After 24 h, cells were washed twice with warm HBSS and incubated with 10 μM dichlorodihydrofluorescein diacetate (DCF) for 40 min. Cells were washed twice in HBSS, and epifluorescent green and red channel images were acquired with cells in an adherent state to avoid perturbation of integrin activity. DCF fluorescence of DsRed-expressing cells was quantified in 16-bit resolution using Metamorph software. The mean of at least 20 cells per chamber in 10 chambers was quantified for each condition.

5-IAF labeling

Oxidation of protein tyrosine phosphatase acidic cysteine residues was assessed as described previously (Wu et al., 1998). Phoenix-293 cells were cotransfected with Flag–PTP-PEST and either empty vector or Myr-TRAF4. After lysis, extracts were labeled with 5 μM 5-IAF (Invitrogen) at 4°C for 60 min, immunoprecipitated with anti-Flag, and immunoblotted with rabbit antifluorescein (Invitrogen). MKP-1 and SHP-2 (SH-PTP2) were similarly immunoprecipitated (Santa Cruz Biotechnology, Inc.) and subjected to immunoblot with antifluorescein.

Online supplemental material

Fig. S1 shows that TRAF4-GFP colocalizes with DsRed-zyxin in focal complexlike structures. Fig. S2 shows that TRAF4-GFP colocalizes with DsRed-zyxin in TIRF microscopy. Fig. S3 shows that TRAF4 concentrates in low density detergent-insoluble membrane fractions. Fig. S4 shows examples of Myr-TRAF4–induced PAK1-dependent cytoskeletal collapse. Fig. S5 shows that Raft disruption decreases Myr-TRAF4–induced ruffling. Online supplemental material is available at http://www.jcb.org/cgi/content/full/jcb.200507004/DC1.

We thank Ginny Poffenberger for expert technical assistance.

This work was supported by the National Heart, Lung, and Blood Institute (grants R01-HL61897 and R01-HL67256), the National Institute of General Medical Sciences (grant R01-GM67674), the Veterans Administration, and the Robert Wood Johnson Foundation (grant to F.E. Nwariaku).

Submitted: 1 July 2005
Accepted: 3 November 2005

References

Ago, T., H. Nunoi, T. Ito, and H. Sumimoto. 1999. Mechanism for phosphorylation-induced activation of the phagocyte NADPH oxidase protein p47(phox). Triple replacement of serines 303, 304, and 328 with aspartates disrupts the SH3 domain-mediated intramolecular interaction in p47(phox), thereby activating the oxidase. *J. Biol. Chem.* 274: 33644–33653.

Allen, W.E., G.E. Jones, J.W. Pollard, and A.J. Ridley. 1997. Rho, Rac and Cdc42 regulate actin organization and cell adhesion in macrophages. *J. Cell Sci.* 110:707–720.

Angers-Loustau, A., J.F. Cote, A. Charest, D. Dowbenko, S. Spencer, L.A. Lasky, and M.L. Tremblay. 1999. Protein tyrosine phosphatase-PEST regulates focal adhesion disassembly, migration, and cytokinesis in fibroblasts. *J. Cell Biol.* 144:1019–1031.

Avraham, H.K., T.H. Lee, Y. Koh, T.A. Kim, S. Jiang, M. Sussman, A.M. Samarel, and S. Avraham. 2003. Vascular endothelial growth factor regulates focal adhesion assembly in human brain microvascular endothelial cells through activation of the focal adhesion kinase and related adhesion focal tyrosine kinase. *J. Biol. Chem.* 278:36661–36668.

Beningo, K.A., M. Dembo, I. Kaverina, J.V. Small, and Y.L. Wang. 2001. Nascent focal adhesions are responsible for the generation of strong propulsive forces in migrating fibroblasts. *J. Cell Biol.* 153:881–888.

Cha, G.H., K.S. Cho, J.H. Lee, M. Kim, E. Kim, J. Park, S.B. Lee, and J. Chung. 2003. Discrete functions of TRAF1 and TRAF2 in *Drosophila melanogaster* mediated by c-Jun N-terminal kinase and NF-kappaB-dependent signaling pathways. *Mol. Cell. Biol.* 23:7982–7991.

Chiarugi, P., G. Pani, E. Giannoni, L. Taddei, R. Colavitti, G. Raugei, M. Symons, S. Borrello, T. Galeotti, and G. Ramponi. 2003. Reactive oxygen species as essential mediators of cell adhesion: the oxidative inhibition of a FAK tyrosine phosphatase is required for cell adhesion. *J. Cell Biol.* 161:933–944.

Cousin, H., and D. Alfandari. 2004. A PTP-PEST-like protein affects alpha5-beta1-integrin-dependent matrix assembly, cell adhesion, and migration in *Xenopus* gastrula. *Dev. Biol.* 265:416–432.

del Pozo, M.A., N.B. Alderson, W.B. Kiosses, H.H. Chiang, R.G. Anderson, and M.A. Schwartz. 2004. Integrins regulate Rac targeting by internalization of membrane domains. *Science.* 303:839–842.

Faust, L.R., J. el Benna, B.M. Babior, and S.J. Chanock. 1995. The phosphorylation targets of p47phox, a subunit of the respiratory burst oxidase. Functions of the individual target serines as evaluated by site-directed mutagenesis. *J. Clin. Invest.* 96:1499–1505.

Franco, S.J., M.A. Rodgers, B.J. Perrin, J. Han, D.A. Bennin, D.R. Critchley, and A. Huttenlocher. 2004. Calpain-mediated proteolysis of talin regulates adhesion dynamics. *Nat. Cell Biol.* 6:977–983.

Frost, J.A., A. Khokhlatchev, S. Stippec, M.A. White, and M.H. Cobb. 1998. Differential effects of PAK1-activating mutations reveal activity-dependent and -independent effects on cytoskeletal regulation. *J. Biol. Chem.* 273:28191–28198.

Gu, Y., Y.C. Xu, R.F. Wu, R.F. Souza, F.E. Nwariaku, and L.S. Terada. 2002. TNF alpha activates c-jun amino terminal kinase through p47phox. *Exp. Cell Res.* 272:62–74.

Inagaki, K., T. Yamao, T. Noguchi, T. Matozaki, K. Fukunaga, T. Takada, T. Hosooka, S. Akira, and M. Kasuga. 2000. SHPS-1 regulates integrin-mediated cytoskeletal reorganization and cell motility. *EMBO J.* 19:6721–6731.

Ishino, M., H. Aoto, H. Sasaski, R. Suzuki, and T. Sasaki. 2000. Phosphorylation of Hic-5 at tyrosine 60 by CAKbeta and Fyn. *FEBS Lett.* 474:179–183.

Kamata, H., S. Honda, S. Maeda, L. Chang, H. Hirata, and M. Karin. 2005. Reactive oxygen species promote TNFalpha-induced death and sustained JNK activation by inhibiting MAP kinase phosphatases. *Cell.* 120:649–661.

Kheradmand, F., E. Werner, P. Tremble, M. Symons, and Z. Werb. 1998. Role of Rac1 and oxygen radicals in collagenase-1 expression induced by cell shape change. *Science.* 280:898–902.

Kiosses, W.B., R.H. Daniels, C. Otey, G.M. Bokoch, and M.A. Schwartz. 1999. A role for p21-activated kinase in endothelial cell migration. *J. Cell Biol.* 147:831–844.

Kontaridis, M.I., S. Eminaga, M. Fornaro, C.I. Zito, R. Sordella, J. Settleman, and A.M. Bennett. 2004. SHP-2 positively regulates myogenesis by coupling to the Rho GTPase signaling pathway. *Mol. Cell. Biol.* 24:5340–5352.

Krautkramer, E., S.I. Giese, J.E. Gasteier, W. Muranyi, and O.T. Fackler. 2004. Human immunodeficiency virus type 1 Nef activates p21-activated kinase via recruitment into lipid rafts. *J. Virol.* 78:4085–4097.

Krylyshkina, O., K.I. Anderson, I. Kaverina, I. Upmann, D.J. Manstein, J.V. Small, and D.K. Toomre. 2003. Nanometer targeting of microtubules to focal adhesions. *J. Cell Biol.* 161:853–859.

Labrecque, L., I. Royal, D.S. Surprenant, C. Patterson, D. Gingras, and R. Beliveau. 2003. Regulation of vascular endothelial growth factor receptor-2 activity by caveolin-1 and plasma membrane cholesterol. *Mol. Biol. Cell.* 14:334–347.

Lacalle, R.A., E. Mira, C. Gomez-Mouton, S. Jimenez-Baranda, A.C. Martinez, and S. Manes. 2002. Specific SHP-2 partitioning in raft domains triggers integrin-mediated signaling via Rho activation. *J. Cell Biol.* 157:277–289.

Lee, H., D.S. Park, X.B. Wang, P.E. Scherer, P.E. Schwartz, and M.P. Lisanti. 2002. Src-induced phosphorylation of caveolin-2 on tyrosine 19. Phospho-caveolin-2 (Tyr(P)19) is localized near focal adhesions, remains associated with lipid rafts/caveolae, but no longer forms a high molecular mass hetero-oligomer with caveolin-1. *J. Biol. Chem.* 277:34556–34567.

Li, Z., M. Hannigan, Z. Mo, B. Liu, W. Lu, Y. Wu, A.V. Smrcka, G. Wu, L. Li, M. Liu, et al. 2003. Directional sensing requires G beta gamma-mediated PAK1 and PIX alpha-dependent activation of Cdc42. *Cell.* 114:215–227.

Litvak, V., D. Tian, Y.D. Shaul, and S. Lev. 2000. Targeting of PYK2 to focal adhesions as a cellular mechanism for convergence between integrins and G protein-coupled receptor signaling cascades. *J. Biol. Chem.* 275:32736–32746.

Liu, H., Y.C. Su, E. Becker, J. Treisman, and E.Y. Skolnik. 1999. A *Drosophila* TNF-receptor-associated factor (TRAF) binds the ste20 kinase Misshapen and activates Jun kinase. *Curr. Biol.* 9:101–104.

Lu, Y., and J. Settleman. 1999. The *Drosophila* Pkn protein kinase is a Rho/Rac effector target required for dorsal closure during embryogenesis. *Genes Dev.* 13:1168–1180.

Lyons, P.D., J.M. Dunty, E.M. Schaefer, and M.D. Schaller. 2001. Inhibition of the catalytic activity of cell adhesion kinase beta by protein-tyrosine phosphatase-PEST-mediated dephosphorylation. *J. Biol. Chem.* 276: 24422–24431.

Manes, S., E. Mira, C. Gomez-Mouton, Z.J. Zhao, R.A. Lacalle, and A.C. Martinez. 1999. Concerted activity of tyrosine phosphatase SHP-2 and focal adhesion kinase in regulation of cell motility. *Mol. Cell. Biol.* 19:3125–3135.

Manser, E., H.Y. Huang, T.H. Loo, X.Q. Chen, J.M. Dong, T. Leung, and L. Lim. 1997. Expression of constitutively active alpha-PAK reveals effects of the kinase on actin and focal complexes. *Mol. Cell. Biol.* 17:1129–1143.

Manser, E., T.H. Loo, C.G. Koh, Z.S. Zhao, X.Q. Chen, L. Tan, I. Tan, T. Leung, and L. Lim. 1998. PAK kinases are directly coupled to the PIX family of nucleotide exchange factors. *Mol. Cell.* 1:183–192.

Matsuya, M., H. Sasaki, H. Aoto, T. Mitaka, K. Nagura, T. Ohba, M. Ishino, S. Takahashi, R. Suzuki, and T. Sasaki. 1998. Cell adhesion kinase beta forms a complex with a new member, Hic-5, of proteins localized at focal adhesions. *J. Biol. Chem.* 273:1003–1014.

McBeath, R., D.M. Pirone, C.M. Nelson, K. Bhadriraju, and C.S. Chen. 2004. Cell shape, cytoskeletal tension, and RhoA regulate stem cell lineage commitment. *Dev. Cell.* 6:483–495.

Meng, T.C., T. Fukada, and N.K. Tonks. 2002. Reversible oxidation and inactivation of protein tyrosine phosphatases in vivo. *Mol. Cell.* 9:387–399.

Moldovan, L., N.I. Moldovan, R.H. Sohn, S.A. Parikh, and P.J. Goldschmidt-Clermont. 2000. Redox changes of cultured endothelial cells and actin dynamics. *Circ. Res.* 86:549–557.

Nishiya, N., Y. Iwabuchi, M. Shibanuma, J.F. Cote, M.L. Tremblay, and K. Nose. 1999. Hic-5, a paxillin homologue, binds to the protein-tyrosine phosphatase PEST (PTP-PEST) through its LIM 3 domain. *J. Biol. Chem.* 274:9847–9853.

Nobes, C.D., and A. Hall. 1995. Rho, rac, and cdc42 GTPases regulate the assembly of multimolecular focal complexes associated with actin stress fibers, lamellipodia, and filopodia. *Cell.* 81:53–62.

Okigaki, M., C. Davis, M. Falasca, S. Harroch, D.P. Felsenfeld, M.P. Sheetz, and J. Schlessinger. 2003. Pyk2 regulates multiple signaling events crucial for macrophage morphology and migration. *Proc. Natl. Acad. Sci. USA.* 100:10740–10745.

Osada, M., T. Ohmori, Y. Yatomi, K. Satoh, S. Hosogaya, and Y. Ozaki. 2001. Involvement of Hic-5 in platelet activation: integrin alphaIIbbeta3-dependent tyrosine phosphorylation and association with proline-rich tyrosine kinase 2. *Biochem. J.* 355:691–697.

Ozaki, M., S.S. Deshpande, P. Angkeow, S. Suzuki, and K. Irani. 2000. Rac1 regulates stress-induced, redox-dependent heat shock factor activation. *J. Biol. Chem.* 275:35377–35383.

Park, S.Y., H.K. Avraham, and S. Avraham. 2004. RAFTK/Pyk2 activation is mediated by trans-acting autophosphorylation in a Src-independent manner. *J. Biol. Chem.* 279:33315–33322.

Regnier, C.H., R. Masson, V. Kedinger, J. Textoris, I. Stoll, M.P. Chenard, A. Dierich, C. Tomasetto, and M.C. Rio. 2002. Impaired neural tube closure, axial skeleton malformations, and tracheal ring disruption in TRAF4-deficient mice. *Proc. Natl. Acad. Sci. USA.* 99:5585–5590.

Ridley, A.J., M.A. Schwartz, K. Burridge, R.A. Firtel, M.H. Ginsberg, G. Borisy, J.T. Parsons, and A.R. Horwitz. 2003. Cell migration: integrating signals from front to back. *Science.* 302:1704–1709.

Rottner, K., A. Hall, and J.V. Small. 1999. Interplay between Rac and Rho in the control of substrate contact dynamics. *Curr. Biol.* 9:640–648.

Sastry, S.K., P.D. Lyons, M.D. Schaller, and K. Burridge. 2002. PTP-PEST controls motility through regulation of Rac1. *J. Cell Sci.* 115:4305–4316.

Tai, L.K., M. Okuda, J. Abe, C. Yan, and B.C. Berk. 2002. Fluid shear stress activates proline-rich tyrosine kinase via reactive oxygen species-dependent pathway. *Arterioscler. Thromb. Vasc. Biol.* 22:1790–1796.

Timpson, P., G.E. Jones, M.C. Frame, and V.G. Brunton. 2001. Coordination of cell polarization and migration by the Rho family GTPases requires Src tyrosine kinase activity. *Curr. Biol.* 11:1836–1846.

Tomasetto, C., C. Regnier, C. Moog-Lutz, M.G. Mattei, M.P. Chenard, R. Lidereau, P. Basset, and M.C. Rio. 1995. Identification of four novel human genes amplified and overexpressed in breast carcinoma and localized to the q11-q21.3 region of chromosome 17. *Genomics.* 28:367–376.

Totsukawa, G., Y. Wu, Y. Sasaki, D.J. Hartshorne, Y. Yamakita, S. Yamashiro, and F. Matsumura. 2004. Distinct roles of MLCK and ROCK in the regulation of membrane protrusions and focal adhesion dynamics during cell migration of fibroblasts. *J. Cell Biol.* 164:427–439.

Turner, C.E., M.C. Brown, J.A. Perrotta, M.C. Riedy, S.N. Nikolopoulos, A.R. McDonald, S. Bagrodia, S. Thomas, and P.S. Leventhal. 1999. Paxillin LD4 motif binds PAK and PIX through a novel 95-kD ankyrin repeat, ARF-GAP protein: A role in cytoskeletal remodeling. *J. Cell Biol.* 145:851–863.

Ushio-Fukai, M., Y. Tang, T. Fukai, S.I. Dikalov, Y. Ma, M. Fujimoto, M.T. Quinn, P.J. Pagano, C. Johnson, and R.W. Alexander. 2002. Novel role of gp91(phox)-containing NAD(P)H oxidase in vascular endothelial growth factor-induced signaling and angiogenesis. *Circ. Res.* 91:1160–1167.

Vilhardt, F., and B. Van Deurs. 2004. The phagocyte NADPH oxidase depends on cholesterol-enriched membrane microdomains for assembly. *EMBO J.* 23:739–748.

Webb, D.J., K. Donais, L.A. Whitmore, S.M. Thomas, C.E. Turner, J.T. Parsons, and A.F. Horwitz. 2004. FAK-Src signalling through paxillin, ERK and MLCK regulates adhesion disassembly. *Nat. Cell Biol.* 6:154–161.

Wu, R.F., Y. Gu, Y.C. Xu, F.E. Nwariaku, and L.S. Terada. 2003. Vascular endothelial growth factor causes translocation of p47phox to membrane ruffles through WAVE1. *J. Biol. Chem.* 278:36830–36840.

Wu, R.F., Y. Gu, Y.C. Xu, S. Mitola, F. Bussolino, and L.S. Terada. 2004. Human immunodeficiency virus type 1 Tat regulates endothelial cell actin cytoskeletal dynamics through PAK1 activation and oxidant production. *J. Virol.* 78:779–789.

Wu, Y., K.S. Kwon, and S.G. Rhee. 1998. Probing cellular protein targets of H2O2 with fluorescein-conjugated iodoacetamide and antibodies to fluorescein. *FEBS Lett.* 440:111–115.

Xu, Y.C., R.F. Wu, Y. Gu, Y.S. Yang, M.C. Yang, F.E. Nwariaku, and L.S. Terada. 2002. Involvement of TRAF4 in oxidative activation of c-jun amino terminal kinase. *J. Biol. Chem.* 277:28051–28057.

Zhao, Z.S., E. Manser, T.H. Loo, and L. Lim. 2000. Coupling of PAK-interacting exchange factor PIX to GIT1 promotes focal complex disassembly. *Mol. Cell. Biol.* 20:6354–6363.